An Ultrawideband Time Reversal-based RADAR for Microwave-range Imaging in Cluttered Media

Lucio Bellomo, Marc Saillard, Sebastien Pioch, K. Belkebir, P. C. Chaumet

An Ultrawideband Time Reversal-based RADAR for Microwave-range Imaging in Cluttered Media

Lucio Bellomo
Marc Saillard
and Sébastien Pioch
LSEET, UMR CNRS 6017
Université du Sud Toulon-Var
Bât. F, BP 20132, 83957 La Garde Cedex, France
Email: {bellomo, saillard, pioch}@lseet.univ-tln.fr

Kamal Belkebir
and Patrick Chaumet
Institut Fresnel, UMR CNRS 6133
Campus de Saint Jérôme, case 162, 13397 Marseille Cedex 20, France
Email: {kamal.belkebir, patrick.chaumet}@fresnel.fr

***Abstract*—This work presents a new RADAR prototype built for the purpose of imaging targets located in a cluttered environment. The system is capable of performing Phase Conjugation experiments in the ultrawideband [2-4] GHz. In addition, applying the D.O.R.T. method to the inter-element matrix allows us to selectively focus onto targets, hence reducing the clutter contribution. We aim to experimentally explore the use of this focusing wave into an inversion algorithm, in order to improve its robustness against noise. Before testing this idea, we show here the first results validating the prototype separately in the frame of selective focusing *via* the DORT method and of multistatic-multifrequency inversion.**

I. Introduction

Using electromagnetic waves for the characterization of otherwise inacessible objects is of interest in many applicative contexts where non-invasive and non-destructive investigations are required, such as for instance medical imaging, geophysical and geological probing, etc. With this purpose, robust nonlinear inversion algorithms minimizing the difference between the measured scattered field and the one relative to the reconstructed objects have been built. In [1], [2] experimental time-harmonic data have been succesfully inversed through a number of such schemes.

Nevertheless the inverse scattering problem is known to be ill-posed and not to have a unique solution. Therefore any clutter present in the investigation region might have a strong impact on the final result. One way to reduce this effect consists in using within the inversion algorithm the response of the scatterer to an incident field focusing onto it. The Time Reversal [3] technique and, more specifically, the DORT method [4] have in the last decade proven to be very effective for this purpose [5].

The DORT method has succesfully been used as a regularization term in an inversion scheme [6], as applied to synthetic data in a buried-object configuration. In order to experimentally prove these results and further explore the potential of the approach, a Time Reversal RADAR is presently under construction. The system consists in a linear array of 8 antennas plus one more spare antenna working in the ultrawideband [2-4] GHz. Besides recording the 8×8 inter-element matrix, the prototype can physically re-emit the focusing wave issued from the DORT method, so that the medium response to it can also be measured and eventually included in the inversion process.

This paper first describes the adopted inversion scheme and its proposed DORT regularization. Then, some preliminary experimental results validating the RADAR are presented. They include an experiment demonstrating the use of DORT for focusing onto a target and an inversion result not yet integrating the DORT contribution. More advanced results including DORT regularization in the framework of inverse scattering will be presented at the conference.

II. Inversion Procedure Including DORT term

The two-dimensional inverse scattering problem is stated in the frequency domain, where for each frequency ω_p, $p = 1, \ldots, P$ and for each illuminating source $j = 1, \ldots, J$, the scattering problem may be formulated as two coupled contrast-source integral equations involving the total electric field $E_{j,p}$ and the contrast distribution $\chi_p(\mathbf{r}) = \varepsilon_{r;p}(\mathbf{r}) - 1$, with $\varepsilon_{r;p}$ being the complex relative permittivity. For the sake of simplicity, symbolic operator notations are used:

$$E^{\mathrm{d}}_{j,p} = \mathbf{G}^{\Gamma}_{j,p} \chi_p E_{j,p}, \tag{1}$$

$$E_{j,p} = E^{\mathrm{inc}} + \mathbf{G}^{\Omega}_{j,p} \chi_p E_{j,p}, \tag{2}$$

where E, E^{inc}, and E^{d} denote the total, incident, and scattered fieds, respectively. $\mathbf{G}^{U=\Gamma,\Omega}$ represents an integral operator whose kernel involves the two-dimensional free space Green function. The aim is to determine the permittivity distribution in a bounded box Ω, such that the corresponding scattered field matches the one measured along a measurement line Γ, $E^{\mathrm{d;meas}}$. An iterative approach is used to solve this ill-posed and nonlinear problem [7]. In this approach, starting from an initial guess, the parameter of interest, i.e. the permittivity distribution, is gradually adjusted by minimization of a cost

function $\mathcal{F}$ of the form

$$\mathcal{F}(E_{j,p};\chi_p) = \frac{\sum_{j=1}^{J}\sum_{p=1}^{P}||h_{j,p}^{(1)}||_{\Omega}^2}{\sum_{j=1}^{J}\sum_{p=1}^{P}||E_{j,p}^{\mathrm{inc}}||_{\Omega}^2} + \frac{\sum_{j=1}^{J}\sum_{p=1}^{P}||h_{j,p}^{(2)}||_{\Gamma}^2}{\sum_{j=1}^{J}\sum_{p=1}^{P}||E_{j,p}^{\mathrm{d;meas}}||_{\Gamma}^2} \quad (3)$$

where the residual errors $h^{(1)}$ and $h^{(2)}$ are defined as follows:

$$h^{(1)} = E_{j,p}^{\mathrm{inc}} - E_{j,p} + \mathbf{G}_{j,p}^{\Omega}\chi_p E_{j,p}, \quad (4)$$

$$h^{(2)} = E_{j,p}^{\mathrm{d;meas}} - \mathbf{G}_{j,p}^{\Gamma}, \chi_p E_{j,p}. \quad (5)$$

Thanks to the DORT method [4] one can retrieve the amplitude and phase laws needed by the array to generate a wave focusing onto a target. Such a wave can therefore be considered as an additional incident wave, $E^{\mathrm{inc;DORT}}$, to which is associated the corresponding diffracted field $E^{\mathrm{d;DORT}}$. The idea is then to construct a new cost function $\mathcal{F}^{\mathrm{DORT}}(E_p^{\mathrm{DORT}};\chi_p)$ built exactly as in (3) but based on these DORT fields, and to merge it with the "regular" one as a regularization term:

$$\tilde{\mathcal{F}}(E_{j,p}, E_p^{\mathrm{DORT}};\chi_p) = \mathcal{F}(E_{j,p};\chi_p)\cdot\mathcal{F}^{\mathrm{DORT}}(E_p^{\mathrm{DORT}};\chi_p). \quad (6)$$

Although this paper does not show results issued from the use of this regularized cost function, it has already been applied succesfully with synthetic data in [6].

To improve the efficiency of the algorithm, we add *a priori* information stating that the desired electrical susceptibility must be greater than unity and that the conductivity must be positive. With these conditions and assuming an Ohmic dispersion model for the materials of interest, the contrast function χ_p reads as

$$\chi_p = \xi^2 + i\frac{\eta^2}{\omega_p\varepsilon_0}. \quad (7)$$

The minimization of the cost function (6) with respect to ξ and η is accomplished using a modified gradient-like method [7].

III. RADAR Description and Preliminary Results

The architecture of our RADAR (Fig. 1) is built around a 2-port Vector Network Analyzer serving both as signal source and receiver. The RF front-end is made of a linear array of 8 UWB antennas (A_1-A_8) plus one more spare antenna (A_9). They are antipodal symmetric Exponentially Tapered Slot (ETS) antennas [8] radiating a vertically-polarized (direction perpendicular to the plane of Fig. 1) electric field. To be able to experimentally re-transmit a focusing wave, each array channel is controlled both in amplitude and phase *via* wideband attenuator/phase shifter (A/Φ) couples driven numerically. Antennas and phase shifters respectively impose the low and high boundaries of the exploitable [2-4] GHz frequency band, sampled with a step of 10 MHz. The spacing between the array antennas has been set to 5 cm ($\lambda_{3\ \mathrm{GHz}}/2$) for a best compromise between antenna coupling and spatial sampling of the scattered field. Also, differential measurements (difference between measurements with and without the scatterer in place) are always used in order to further reduce antenna coupling [9].

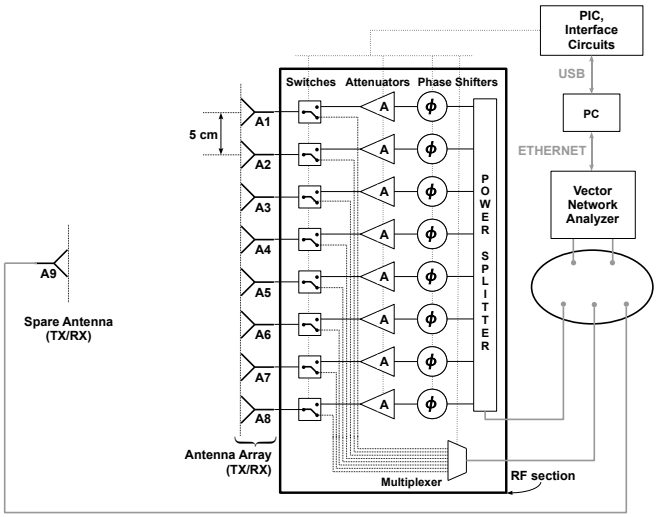

Fig. 1. Prototype architecture.

A. Generation of a focusing wave

One of the experiments we have conducted to validate the prototype consists in applying the DORT method in a configuration with a 4 cm-diameter metallic cylinder located 40 cm away from the array center. The array antennas transmit and receive at turn, to finally build the 8×8 so-called inter-element matrix $\mathbf{K}$ for each of the available frequencies. The DORT method consists in extracting the principal components of the recorded field through a Singular Value Decomposition (SVD) of $\mathbf{K}$: the singular values provide informations on the number of scatterers and on their scattering strenghts, whereas the associated singular vectors represent a normalized version of the field components associated to the scatterers as recorded by the array antennas [4], [5]. In Fig. 2(a) we have plotted the three largest singular values versus frequency. The largest one, clearly emerging from the others, is effectively associated to the isotropic component of the field scattered from the target, so that the corresponding singular vector supplies the amplitude and phase laws needed to generate a wave focusing onto it. We have experimentally coded such vector at each frequency into the system and we have measured the object response to the focusing wave. Switching to the time domain through a Fourier transform, we have also simulated the propagation of the focusing wave and built a chart of the field over the area of interest. Here, the antennas are simply modeled as vertical electric dipoles. The frame at the instant when the wave converges onto the cylinder is given in Fig. 2(b), where one can appreciate the focusing of the wave onto the target. The cross-range resolution (half of the focusing region along the direction parallel to the array) is $\approx$

8 cm, in accordance with the theoretical limit $\lambda F/D$, where F is the distance between the array and the target (40 cm), D is the array aperture (35 cm) and λ is here the wavelength at the highest frequency 4 GHz (7.5 cm) [10].

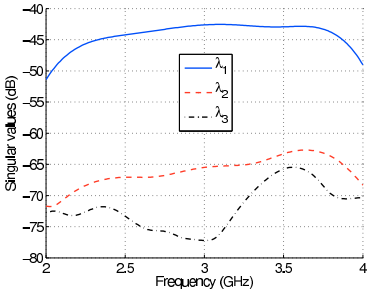

(a)

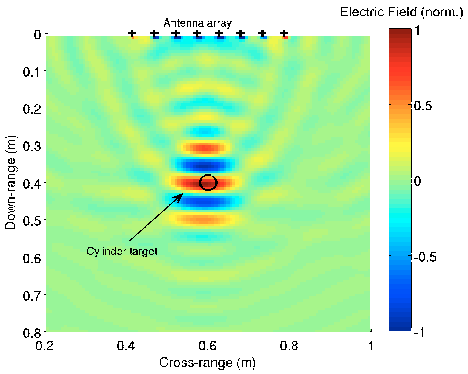

(b)

Fig. 2. UWB DORT experiment. (a) Array inter-element matrix singular values distribution versus frequency and (b) one frame of the synthetic time-domain field chart movie associated to the largest eigenvalue.

B. Inverse Scattering

We have started testing the RADAR in the framework of 2D inverse scattering. The configuration is depicted in Fig. 3. The target is the same metallic cylinder as above, located in front of antenna A_5. Notice the small array aperture angle, $\approx 34°$.

1) Calibration of the Incident Field: First of all, an accurate calibration of the incident field is required. Our setup is such that the outer antennas (e.g. A_1 and A_8) do not illuminate the target in the forward direction, but with incidence angles up to $\approx 20°$. This, in conjunction with the anisotropic antenna radiation patterns, make an accurate incident field modeling compulsory.

For calibration purpose, we place the spare antenna A9 in front of the array at the center of the test region Ω (Fig. 3). The radiated field measured by each antenna A_j of the array is stored in the vector of transmission S-parameters $\mathbf{S}^{\text{cal}}$, whose j^{th} component S^{cal}_{j9}, $j = 1, \ldots, J = 8$ is recorded at each frequency ω_p, $p = 1, \ldots, P = 201$ in the [2-4] GHz band (we drop from here on the subscript p for lighter notations). Then, as in [11], we use a Fourier expansion to model the

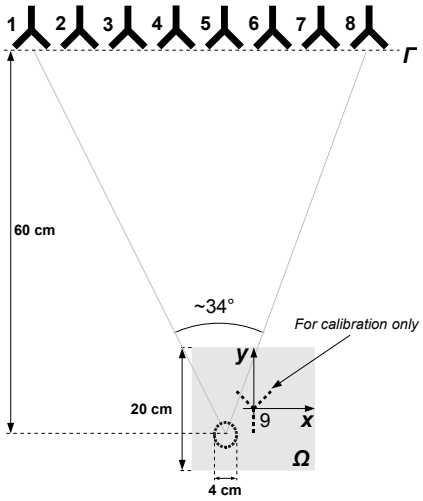

Fig. 3. Experimental configuration of the inverse scattering problem.

radiation pattern:

$$S^{\text{cal}}_{j9} = \sum_{n=-N}^{N} \gamma_n H_n^-(kr_{j9}) e^{-in\theta_{j9}}, \quad j = 1, \ldots, 8 \qquad (8)$$

or, with a matrix notation,

$$\mathbf{S}^{\text{cal}} = \mathbf{H}\boldsymbol{\Gamma}, \qquad (9)$$

where k is the wave number in free-space at the p^{th} frequency, γ_n is the n^{th} unknown coefficient, H_n^- is the Hankel function of second kind of order n and r_{j9} and θ_{j9} are the polar coordinates of the vector going from A_9 to A_j (Fig. 3).

The choice of the truncation order N is delicate: if too high, the highest coefficients of $\mathbf{S}^{\text{cal}}$ are corrupted by noise and can affect the solution of the inversion algorithm, whereas if it is too low, it fails at modeling the pattern away from the forward direction. Plotting the γ_n, it appears that they decrease rapidly for $N > 1$, so that $N = 1$ is a choice well suited for our experimental setup. Eq. (9) can finally be solved for $\boldsymbol{\Gamma}$ by computing the pseudo-inverse of $\mathbf{H}$ through its SVD [11].

One must notice though that in (9) $\boldsymbol{\Gamma}$ is experimentally related to the radiation pattern of *both* A9 and the array antennas, that is, the transmitting and receiving antennas. Nevertheless, in [7], [11] it is used to model the incident field only. We propose to split it in two by introducing a new quantity, the *effective length* of an antenna $l_{\text{e}}(r, \theta)$, which we lend from classical Antenna Theory [12] where it is used to describe the far-field radiation pattern of an antenna. Under the assumption that the antennas are all identical, for each point in Ω and for each antenna we can express the antenna radiation pattern as a function of the square of l_{e}:

$$\sum_{n=-N}^{N} \gamma_n H_n^-(kr_j) e^{-in\theta_j} = l_{\text{e}}^2(r_j, \theta_j) H_0^-(kr_j), \qquad (10)$$

where r_j and θ_j are the polar coordinates of the vector going from A_j to the chosen point. Notice that even though A_9 is the same ETS antenna than the eigth array antennas, the latter

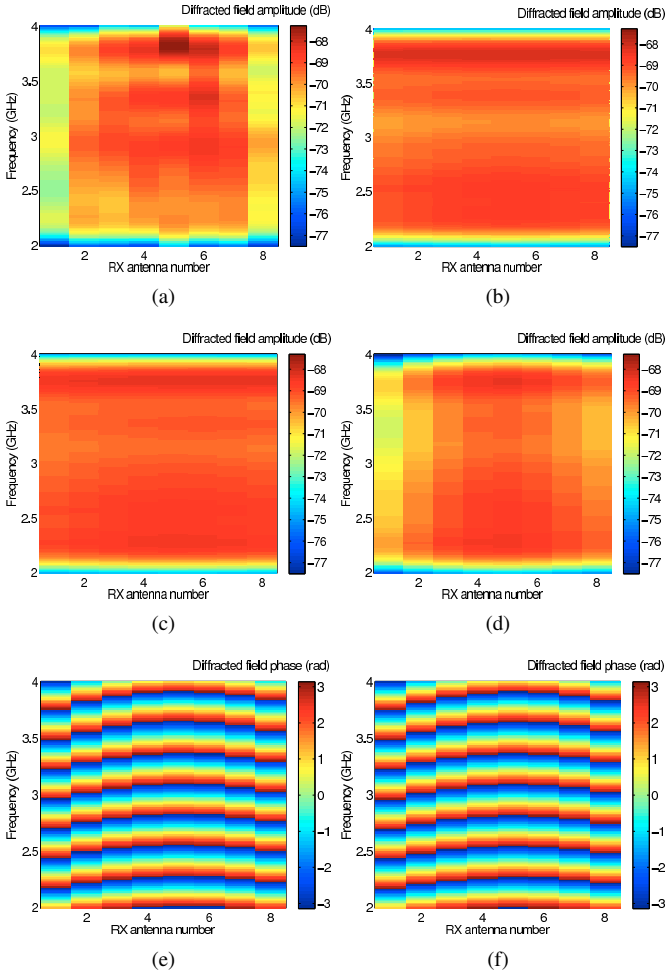

Fig. 4. (a-d) Amplitude and (e-f) phase of the diffracted field as a function of the frequency and of the number of the receiving antenna in the case of antenna A_5 used as emitter. (a,e) Measurement; simulation with incident field calibration based on a (b) monopolar, (c) multipolar ($N = 1$) and (d,f) multipolar/effective length expansion.

are mutually coupled because of their proximity, so that their radiation pattern can not be identical to the one of A_9: in this sense a further assumption is used in writing (10).

Once all the $l_e(r_j, \theta_j)$ have been determined from (10), the incident field for the transmitting antenna A_j and the Green function operator in (1) and (2) are approximated by

$$E_j^{\text{inc}} = l_e(r_j, \theta_j) H_0^-(kr_j) \tag{11}$$

and

$$\tilde{\mathbf{G}}_j^{\Gamma} = l_e(r_j, \theta_j) \mathbf{G}_j^{\Gamma} \tag{12}$$

respectively, thus creating two separate transmission and reception antenna radiation patterns. Except from these "initial" modifications, the inversion algorithm remains unchanged.

In order to appreciate the impact of this calibration strategy, we have simulated the scattered field associated to the problem depicted in Fig. 3 with the domain integral formalism. Using A_5 as transmitting antenna, Fig. 4 shows the comparison between the measured and the simulated scattered fields as a function of the frequency (vertical axis) and of the number of the receiving antenna (horizontal axis). The effect of the calibration is quite obvious when amplitude is concerned: measurements are reported in Fig. 4(a), whereas the next three plots depict the simulated results for three different calibration methods: (b) a monopolar ($N = 0$ in (8)) and (c) a multipolar ($N = 1$) expansion applied to the incident field model without splitting $\mathbf{\Gamma}$ in transmission and reception effective lengths, and (d) the same multipolar expansion but including the concept of effective length as in (10). It is noticed that the last technique outperforms the two others because it is the only technique that appropriately models the reception gain of the outer antennas, which indeed "see" the target away from the forward direction. The phase modeling is less critical and all methods give an excellent phase matching between measurements and simulations. Here, we only report the result when the effective lengths are used (Fig. 4(f)).

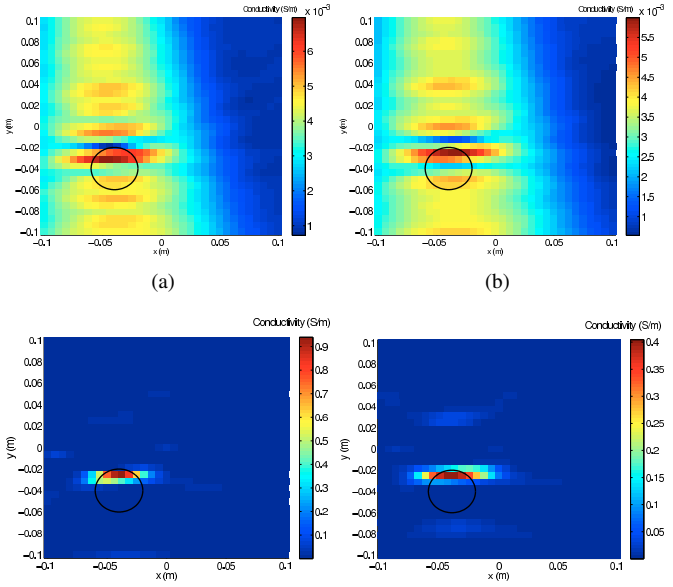

Fig. 5. Distribution of the reconstructed conductivity from (a,c) synthetic and (b,d) experimental data. (a) and (b) are the initial estimates retrieved throught the backpropagation method, (c) and (d) show the final result.

2) Reconstruction Results: The inverse problem is based on the algorithm previously described but does not include the response to the DORT focusing wave yet. We look for the real and imaginary permittivity profiles in the 20 cm $\times$ 20 cm test region Ω, discretized with a step of $\sim$0.65 cm ($\sim \lambda_{3\ \text{GHz}}/15$), and no assumption is made about the material (dielectric, conductor) of the target. The initial guess, derived from the backpropagation method [13], is shown in Fig. 5 (a) and (b) for synthetic and experimental data, respectively; the conductivity distributions provided by the inversion scheme after the iterative algorithm has converged are in Fig. 5 (c) and (d). In the experimental case, the effective length calibration technique is applied. The real part of the permittivity is not shown since it is noisy and small-valued everywhere in Ω. The small array aperture and the impenetrable nature of the object are such that we cannot image the back of the object,

as confirmed by the inversion from noiseless synthetic data, which match that from measurements very well, except that the maximum of conductivity reaches 0.9 S/m instead of 0.4 S/m.

IV. Conclusion and Perspectives

We have manufactured a Time Reversal RADAR prototype working in the [2-4] GHz frequency band. Its validation has been initially accomplished in the context of the DORT method used for generating a wave selectively focusing onto a target. In the framework of 2D inverse scattering, we have succesfully imaged a metallic cylinder despite its non-infinite height and the unmodeled anistropic radiation pattern of the antennas along the vertical axis, thus showing the imaging capabilities of our multistatic-multifrequency configuration.

We wish now to merge the two approaches in order to increase the inversion algorithm robustness in cluttered media by adding to the inversion process the response to the DORT focusing wave. We are currently building a second antenna array that will indeed allow us to measure such response, so that the first experimental results will be presented at the conference.

Acknowledgment

This work is supported by DGA/CNRS. The ETS antennas have been kindly offered by LEAT in Nice-Sophia Antipolis, France.

References

[1] K. Belkebir and M. Saillard, "Special section: Testing inversion algorithms against experimental data," *Inverse Problems*, vol. 17, no. 6, pp. 1565–1571, Dec. 2001.

[2] ——, "Special section on testing inversion algorithms against experimental data: inhomogeneous targets," *Inverse Problems*, vol. 21, no. 6, pp. S1–S3, Dec. 2005.

[3] M. Fink, C. Prada, F. Wu, and D. Cassereau, "Self focusing in inhomogeneous media with time reversal acoustic mirrors," in *Proc. IEEE Ultrasonics Symposium*, vol. 2, Montreal, Que., Canada, Oct. 1989, pp. 681–686.

[4] C. Prada and M. Fink, "Eigenmodes of the time reversal operator: A solution to selective focusing in multiple-target media," *Wave Motion*, vol. 20, pp. 151–163, Sep. 1994.

[5] G. Micolau and M. Saillard, "D.O.R.T. method as applied to electromagnetic subsurface sensing," *Radio Sci.*, vol. 38, no. 3, pp. S63–S79, May 2003.

[6] A. Dubois, K. Belkebir, and M. Saillard, "Localization and characterization of two-dimensional targets buried in a cluttered environment," *Inv. Probl.*, vol. 20, no. 6, pp. S63–S79, Nov. 2004.

[7] ——, "Retrieval of inhomogeneous targets from experimental frequency diversity data," *Inverse Problems*, vol. 21, no. 6, pp. S65–S79, Dec. 2005.

[8] E. Guillanton, J. Y. Dauvignac, C. Pichot, and J. Cashman, "A new design tapered slot antenna for ultra-wideband applications," *Microwave and Optical Technology Letters*, vol. 19, no. 4, pp. 286–289, 1998.

[9] A. Cresp, I. Aliferis, M. J. Yedlin, J.-Y. Dauvignac, and C. Pichot, "Time-domain processing of electromagnetic data for multiple-target detection," *AIP Conf. Proc., 3rd Conference on Mathematical Modeling of Wave Phenomena*, vol. 1106, no. 1, pp. 204–213, Mar. 2009.

[10] M. Born and E. Wolf, *Principles of Optics*, 1970.

[11] D. Franceschini, M. Donelli, and A. Massa, "On the effects of the electromagnetic source modeling in the iterative multiscaling method," *Radio Sci.*, vol. 42, p. RS3020, Jun. 2007.

[12] D. M. Pozar, *Microwave engineering*, 2nd ed., 1998, pp. 206–208.

[13] R. E. Kleinman and P. M. van den Berg, "Two-dimensation location and shape reconstruction," *Radio Sci.*, vol. 29, no. 4, pp. 1157–1169, 1994.

ANSWERS TO COMMENTS

Both reviewers have pointed out that we do not clearly state since the early stages of the paper that we do not present experimental results issued from the DORT incident field applied to the inversion algorithm. This was indeed a fruitful remark, and we have made it clear both in the abstract and in the introduction that we only present results validating the prototype *separately* in the frame of DORT method used for focusing and in the frame of inverse scattering. In addition, the conclusion explicitly underlines the fact that we are currently working on the DORT incident field technique since we are about to acquire a second antenna array necessary to measure the response to such a focusing wave.

More specific comments have been given in the review paper entitled `PR_74_BELLOMO_LUCIO_rev_0_104.doc`.

- Formulas (4) and (5) have been corrected.
- DORT method has been described with more details in Section III. References [4], [5] have also been cited for an accurate review of the method.
- Again in Section III, the statement "excellent focusing" has been reformulated by stressing the fact that the resolution we obtain corresponds very well to the theoretical one [10].
- Equation (10) is based on the assumption that the antennas are all identical. In a sense, through this formulation we reconstruct the *actual* radiation pattern of the antennas, modified as it is by mutual coupling. Nevertheless, we have pointed out that this assumption is not completely verified in our setup, since the antenna A_9 (used as source for the calibration task) is not mutually coupled to any of the other antennas, hence its effective length is in effect not exactly the same as that of all the other antennas.
- The backpropagation result, used as initial estimate for the inversion algorithm, has been added to the paper.

Finally, both reviewers have suggested that we present the reconstruction of a penetrable object instead of a metallic one. Unfortunately, the very low array aperture angle (see Fig. 3) is such that an extended (with respect to the wavelength) penetrable object is not properly reconstructed. As an example, the figure below shows the experimental reconstruction of a wooden ($\Re\{\epsilon_r\} \approx 1.5$) 2D object whose section is a rectangle of dimensions 7 cm $\times$ 10.5 cm ($0.7\lambda \times 1.05\lambda$ at 3 GHz in vacuum); it is placed at a distance of 50 cm from the array in front of A_5. We do not present the results from synthetic data since they are not fundamentally different from those in Fig. 6. Indeed, the array aperture is so low that only the edges which are parallel to tha antenna array are reconstructed, and the algorithm does not even cleary distinguishes their dielectric nature from the conducting one. The experimental results about the metallic object in Fig. 5 are simply meant to prove two facts: that our prototype is able to measure data which are clean enough for an inversion algorithm to give a reasonable result and that the experimental data are properly integrated within the existing algorithm (especially in terms of the incident field calibration procedure).

We now aim to improve our reconstructions (both metallic and dielectric objects) by using a second antenna array which, besides recording the response to the DORT focusing wave, will allow us to increase the overall aperture of our system so to gather richer spatial information on the scattered field.

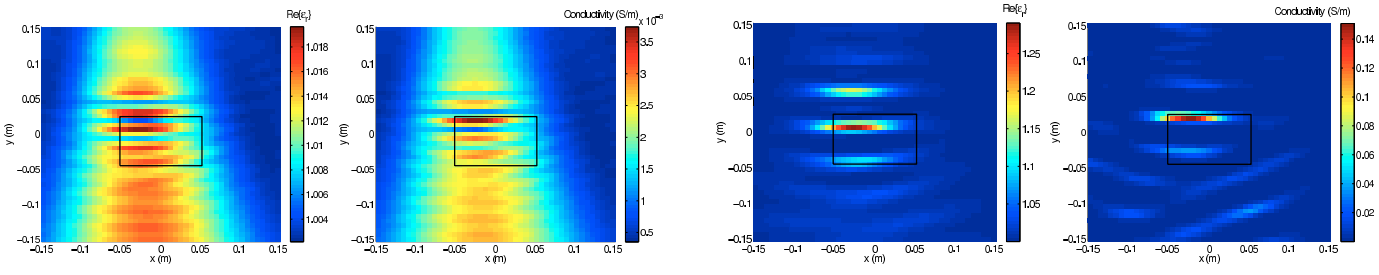

(a) (b) (c) (d)

Fig. 6. Distribution of the reconstructed (a,c) real part of the permittivity and (b,d) conductivity from experimental data. (a) and (b) are the initial estimates retrieved throught the backpropagation method, (c) and (d) show the final result.